analytical chemistry

pubs.acs.org/ac Article

# Hand-Held Raman Spectrometer-Based Dual Detection of Creatinine and Cortisol in Human Sweat Using Silver Nanoflakes

Hyun Soo Kim, Hyun Jung Kim, Jaehun Lee, Taeha Lee, Jongsu Yun, Gyudo Lee,* and Yoochan Hong*

Cite This: *Anal. Chem.* 2021, 93, 14996−15004 Read Online

ACCESS | Metrics & More | Article Recommendations | Supporting Information

**ABSTRACT:** The conventional tissue biopsy method yields isolated snapshots of a narrow region. Therefore, it cannot facilitate comprehensive disease characterization and monitoring. Recently, the detection of tumor-derived components in body fluids—a practice known as liquid biopsy—has attracted increased attention from the biochemical research and clinical application viewpoints. In this vein, surface-enhanced Raman scattering (SERS) has been identified as one of the most powerful liquid-biopsy analysis techniques, owing to its high sensitivity and specificity. Moreover, it affords high-capacity spectral multiplexing for simultaneous target detection and a unique ability to obtain intrinsic biomolecule-fingerprint spectra. This paper presents the fabrication of silver nanosnowflakes (SNSFs) using the polyol method and their subsequent dropping onto a hydrophobic filter paper. The SERS substrate, which comprises the SNSFs and hydrophobic filter paper, facilitates the simultaneous detection of creatinine and cortisol in human sweat using a hand-held Raman spectrometer. The proposed SERS system affords Raman spectrometry to be performed on small sample volumes (2 $\mu$L) to identify the normal and at-risk creatinine and cortisol groups.

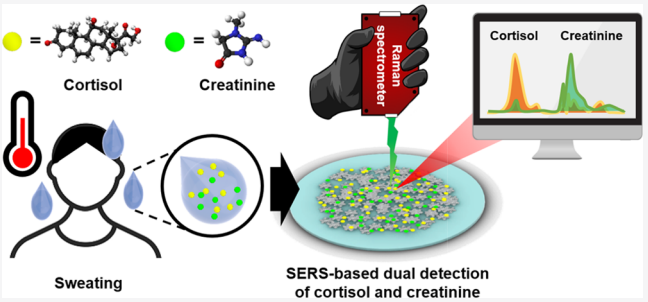




## INTRODUCTION

The use of liquid-biopsy techniques in lieu of the conventional, invasive diagnostic, and examination methods has recently attracted increased research attention.[1] The conventional diagnostic method involves tissue biopsy, which is performed using invasive surgical tools, such as endoscopes and needles. Therefore, they pose injury risks to patients and medical practitioners. In addition, the feasibility of performing a tissue biopsy depends on the location and size of the diseased tissue and patients' health condition.[2] Furthermore, if the diseased region lies between or inside tissues, the concerned biopsy procedure might present doctors with insufficient information for prescribing an appropriate treatment.[3]

To overcome the associated risks and limitations of tissue biopsy, several researchers have actively investigated the use of liquid sampling for screening novel biomarkers and disease diagnosis. Liquid sampling uses human biofluids, such as blood, urine, and sweat. Being non-invasive, non-blood-based liquid-biopsy techniques have received much attention. Human sweat contains several biomarkers, including electrolytes, metal ions, metabolites, amino acids, proteins, and hormones.[4] Creatinine, in particular, serves as an important bioindicator of renal functions and an analyte of interest in the diagnosis of several diseases—dystrophy, thyroid dysfunction, and heatstroke.[5] Cortisol is another biomarker present in sweat, and it is associated with acute and chronic stress conditions. For example, cortisol-related, stress-induced mood disorders cause such mental illnesses as Cushing's syndrome, Addison's disease, bipolar disorders, and depression.[6]

Historically, several conventional methods, including colorimetric assays,[4] fluorescence analysis,[7] and chemiluminescence immunoassays,[8] have been used to detect creatinine and cortisol. In addition, updated analytical methods involving localized surface plasmon resonance-based refractive-index analysis,[9] chemiresistors,[10] and electrochemical sensors[11] have been employed for creatinine and cortisol detection. These methods perform the said detection under predefined physiological conditions; however, they involve complex preparation processes and suffer from low sensitivity, low accuracy, and long detection times. The key characteristics, such as detection limits and detection ranges, of each method are compared and summarized in "Supporting Information" (Table S1). Therefore, effective, high sensitivity, and high-accuracy analytical methods must be developed to address these limitations of existing techniques.

Raman spectroscopy-based analysis can overcome the drawbacks of the aforementioned analytical approaches

Received: June 14, 2021
Accepted: October 26, 2021
Published: November 5, 2021

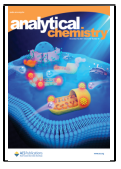




https://doi.org/10.1021/acs.analchem.1c02496
*Anal. Chem.* 2021, 93, 14996−15004

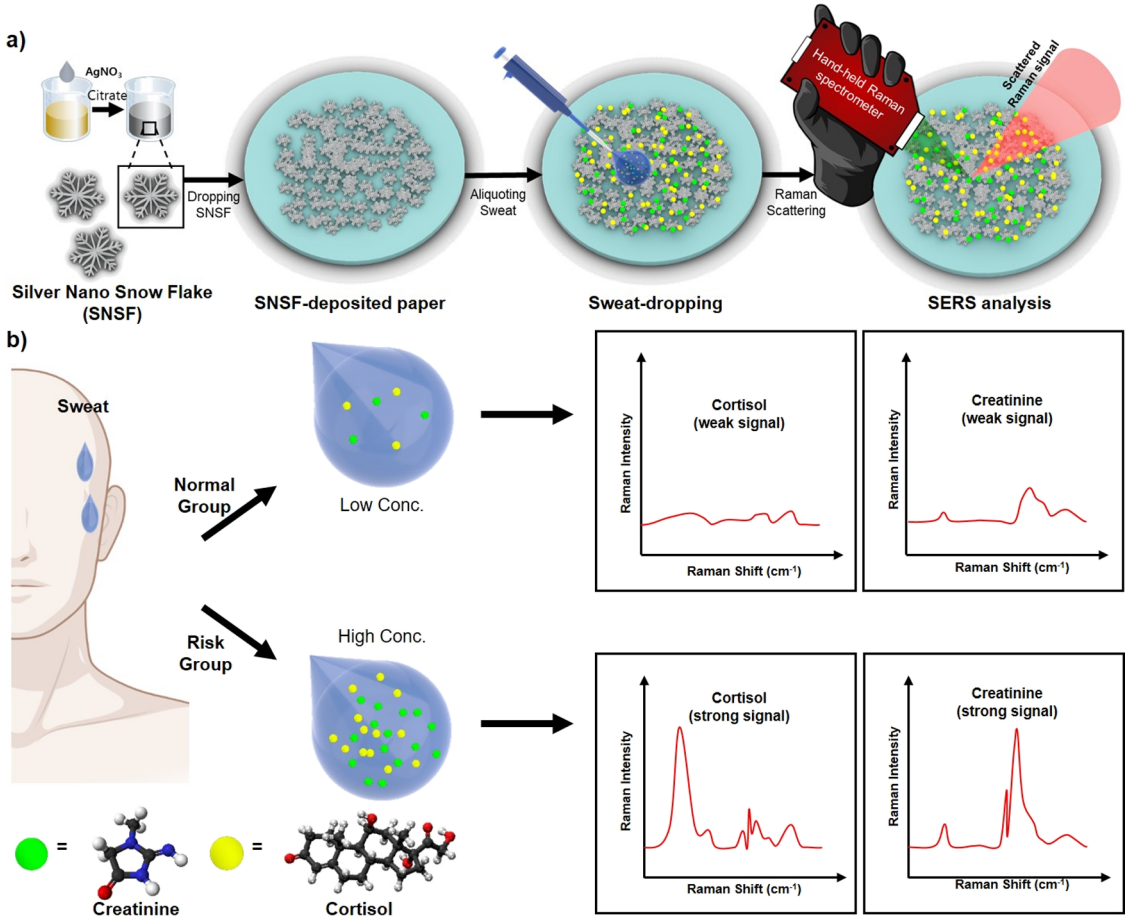


**Figure 1.** (a) Schematic of fabrication and analysis processes for detection of biomarkers in human sweat using a hand-held Raman spectrometer and (b) liquid-biopsy platform for classification of normal and risk groups in human sweat.

because it can rapidly analyze samples in any physical state without destruction.[12] Moreover, the associated instrumentation can be miniaturized to the hand-held scale.[13] Furthermore, the Raman spectra provide highly specific chemical structure fingerprints. The typically weak signals obtained via Raman spectroscopy can be strengthened via surface-enhanced Raman scattering (SERS) that capitalizes on the intrinsic properties of plasmonic metals.[14] The rapid strengthening of the electromagnetic field produced by localized surface plasmons on metal nanostructures facilitates the amplification of Raman signals pertaining to the adsorbed analytes.[15] Although a low spot-to-spot reproducibility might cause variability in the SERS signal strength, this issue can be addressed by modifying the SERS-substrate fabrication technique. For example, electrochemical deposition,[16] vapor deposition,[17] and electron-beam lithography[18] have previously been applied to fabricate reproducible SERS substrates. Although useful, these processes are complex, expensive,[19] and not environmentally friendly. Compared to other commonly used SERS-substrate materials, such as glass, silicon, anodic aluminum oxide, and polydimethylsiloxane, paper comprises ecofriendly cellulose. Moreover, it can be easily shape-controlled and contains hydroxyl groups that are readily functionalized.

This paper presents a method to develop a simple, inexpensive, and easy-to-manufacture SERS substrate to facilitate high-sensitivity, high-accuracy Raman spectroscopy signal measurements. The proposed method involves the use of a silver nanosnowflake (SNSF)-treated hydrophobic filter paper-based SERS substrate and a hand-held Raman spectrometer. The hydrophobic modification of the filter paper surface increases its contact angle, which in turn, increases and decreases the SNSF contact angle and contact area, respectively, thereby facilitating its concentration in a small region. These concentrated SNSFs result in the creation of SERS hot spots. To minimize the spot-to-spot variation in the Raman signal strength, the spatial distribution of SNSFs can be controlled by varying their drop concentrations. Using these SNSFs and the hydrophobic filter paper-based SERS substrates, the relevant Raman spectra can be acquired from standard creatinine and cortisol solutions.

In this study, creatinine and cortisol were spiked into human sweat. Subsequently, the Raman signals acquired for these spiked samples were analyzed to classify the normal and risk groups. Furthermore, this study confirms the simultaneous detection of two biomarkers—creatinine and cortisol—by observing changes in the corresponding Raman signals, owing to changes in the cortisol and creatinine concentration (Figure 1).

## EXPERIMENTAL SECTION

**Materials.** In this study, silver nitrate ($AgNO_3$), hydroxylamine solution (50% w/w in water), trisodium citrate, sodium hydroxide (NaOH), creatinine, and cortisol were purchased from Sigma-Aldrich (USA). Moreover, an alkyl ketene dimer (AKD) was obtained from Solenis (Gimcheon, Korea). The


https://doi.org/10.1021/acs.analchem.1c02496
Anal. Chem. 2021, 93, 14996−15004

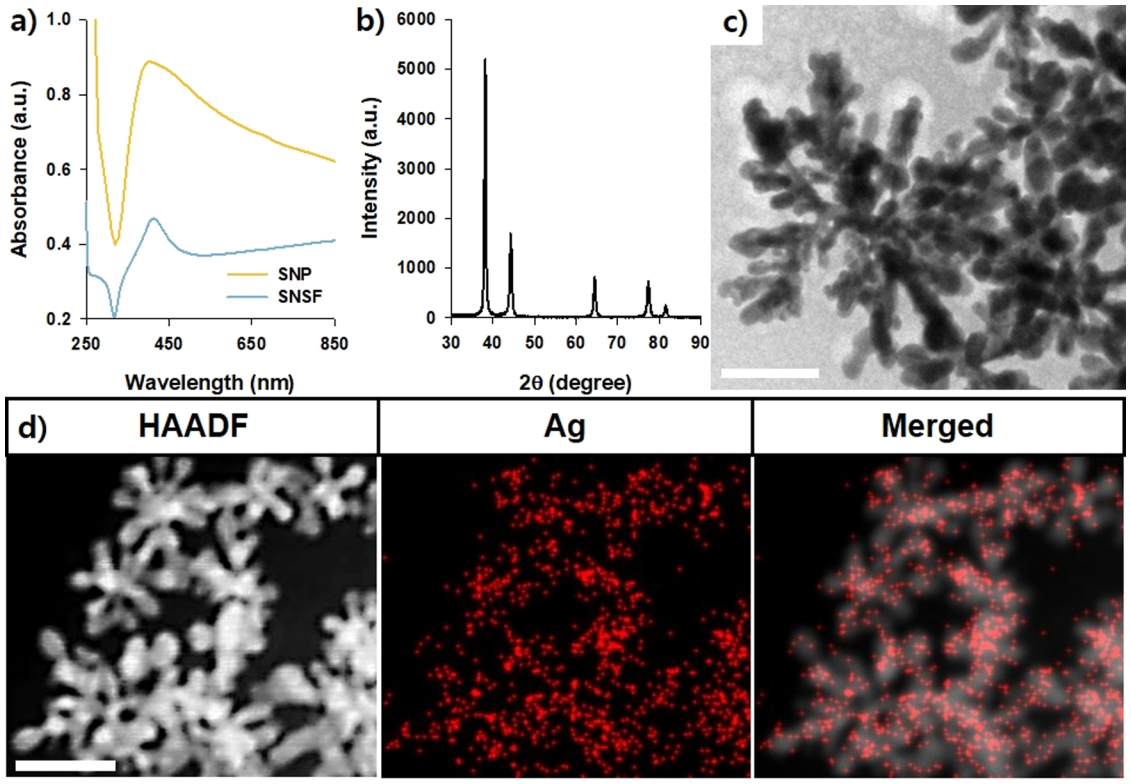


**Figure 2.** (a) Absorbance spectra of SNSFs (blue) and SNP (yellow) synthesized with and without trisodium citrate, respectively, (b) SNSF XRD pattern, (c) field emission transmission electron microscopic image of SNSF (scale represents 100 nm), and (d) high-angle annular dark-field transmission electron microscopic image and energy-dispersive X-ray elemental mapping of the silver content in the final SNSF (scale represents 200 nm).

filter paper was procured from Advantec (grade 5c, USA). All chemicals and reagents used in this study were of analytical grade. Ultrapure deionized (DI) water was used for all synthetic processes.

**Synthesis of SNSF and SNPs.** A colloidal SNSF suspension was synthesized in accordance to a previously reported polyol method[20] with the following modification: hydroxylamine (500 $\mu$L, 60 mM) was mixed with NaOH (500 $\mu$L, 50 mM). Subsequently, $AgNO_3$ (9 mL) was added to the mixture using a syringe pump with a 1 mL/min flow rate. The resulting solution was stirred for 5 min at 500 rpm. Upon completion of the reaction, trisodium citrate (100 $\mu$L, 1% w/v) was added to the mixture with continuous stirring at 500 rpm for 15 min. The resulting solution was subsequently centrifuged using a Centricon filter (molecular-weight cutoff: 3000 Da) for 1 h at 3000 rpm. The supernatant was removed, and the SNSF pellets were redispersed in DI water. The SNPs were similarly synthesized without the administration of trisodium citrate in the final step of the synthetic process.

**Fabrication of Hydrophobic Filter Paper-Based SNSF Raman Substrates.** In this study, the sensitive filter paper-based SNSF substrates were fabricated in accordance to a previously published report.[19] As per this approach, the filter paper was punched to 5 mm diameter samples and soaked in the AKD solution (0.01% v/v) for 5 min. Subsequently, the filter paper was washed with DI water and dried at 70 °C for 1 h. Lastly, 10 $\mu$L of SNSF was dropped onto the AKD-treated filter paper and dried.

**Raman Spectra Measurement.** The Raman spectra were acquired in accordance to a previously published report[21] with modifications. They were collected using 785 nm laser excitation. The NS-100 hand-held Raman spectrometer (Nanoscope Systems Inc.; Daejeon, Korea) was used to this end. During measurements, the laser power was set to 80 mW, and the distance between the sample and hand-held Raman spectrometer was maintained to ensure the realization of a 1 mm laser spot on the SNSF substrate. The integration time was fixed to 10 s. The Raman spectra were collected for 10 different spots on each SNSF substrate sample under identical conditions.

**Preparation of Human Sweat Samples.** The human sweat samples were collected from volunteers and centrifuged using the Centricon filter (molecular-weight cutoff: 10,000) for 30 min at 13,500 rpm. Subsequently, the sweat samples were spiked with specific creatinine and cortisol concentrations, and subsequent analyses were performed.

## RESULTS AND DISCUSSION

**Synthesis SNSF and Characterization.** In this study, after the above-described synthesis of SNSF and SNP, the absorbance spectra were acquired, as described in Figure 2a. As can be seen, the absorbance peaks for both nanoparticles appear near 385 nm; however, the inclusion of trisodium citrate during SNSF fabrication yields an additional absorbance plateau over a wider wavelength range. The SNSF X-ray diffraction (XRD) pattern (Figure 2b) is indicative of a face-centered cubic structure. In addition, all SNSFs demonstrate a similar diffraction profile, and the observed peaks at 38.1, 44.2, 64.7, and 77.4° can be attributed to the 111, 200, 220, and 311 crystallographic planes of the face-centered cubic silver crystals, respectively.[22] Ag represents the main phase, and no other marked phases can be observed, owing to impurities in the


https://doi.org/10.1021/acs.analchem.1c02496
Anal. Chem. 2021, 93, 14996−15004

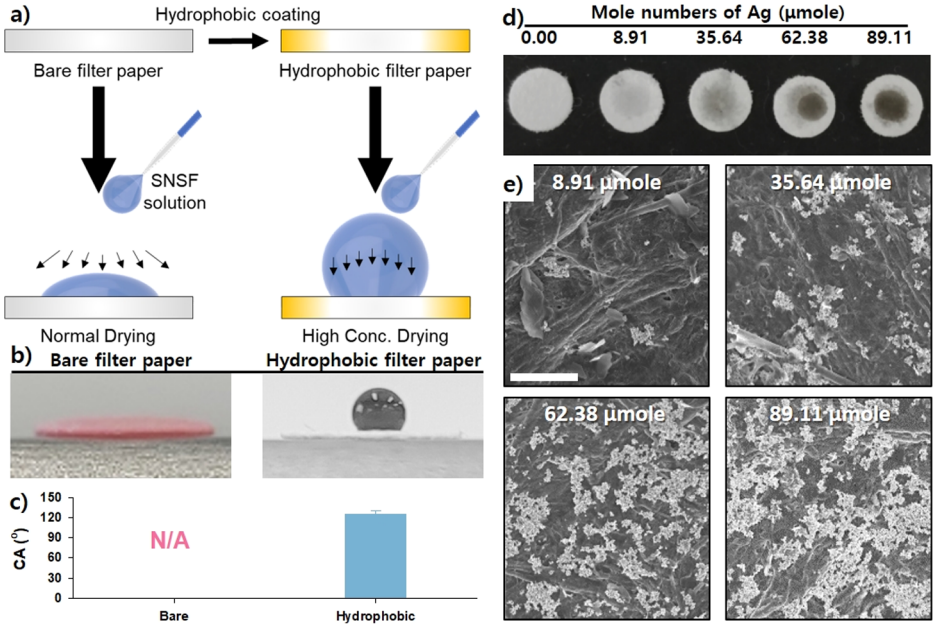


**Figure 3.** (a) Schematic of hydrophobic filter paper-based substrate coating, (b) water droplets placed on bare (left) and hydrophobic (right) filter papers, (c) contact angles of bare and hydrophobic filter paper, (d) SNSF-treated hydrophobic filter paper with indicated mole numbers of Ag, and (e) FE-SEM images of SNSF-treated hydrophobic filter papers (scale represents 5 $\mu$m).

pattern. The substantial SNSF absorbance, as shown in Figure 2a, can be attributed to variations in the SNSF morphology (Figure 2c), which lead to differences in the localized surface plasmon resonances in the suspension over a wide range of visible and near-infrared wavelengths.[20] The average SNSF diameter lies in the 200−400 nm range. As depicted in Figure 2c, the SNSF microstructure is characterized by 7−12 arms extending outward from the core. The average arm count equals 8. The tips of these arms are generally not sharp, and some of arms are branched. Figure 2d depicts the spatial distribution of silver within the SNSFs, as observed via energy-dispersive X-ray elemental mapping. These results indicate that SNSFs exclusively comprise Ag.

**Fabrication of the SERS Substrate and Optimization.** During the fabrication of the proposed SERS substrate, the filter paper hydrophobicity was increased via esterification of cellulose fiber hydroxyl groups in the filter paper with AKD (Figure 3a). Figure 3b depicts photographs of the bare filter paper and one with a single SNSF droplet. While the bare filter paper absorbs the SNSF solution, the AKD-treated hydrophobic filter paper retains the solution as an aqueous droplet on its surface. To confirm the hydrophobicity of the filter paper, its contact angle was measured before and after AKD treatment (Figure 3c). Evidently, the contact angle of the bare filter paper could not be measured, owing to the immediate absorption of the water droplet. However, the contact angle between the water droplet and AKD-treated hydrophobic filter paper was determined to be 125.33 ± 5°. Moreover, the droplet was observed to remain on the surface of the hydrophobic filter paper for up to an hour. Prior studies have established that Raman signals can be strengthened by distributing noble metal nanostructures in close proximity.[21,23] Accordingly, in this study, the SERS effect was optimized by varying the mole numbers of Ag for SNSF on the AKD-treated hydrophobic filter paper (Figure 3d). As depicted in Figure 3e, the SNSF distributions in the filter paper-based SERS substrates with varying Ag mole numbers were confirmed via field-emission scanning electron microscopy. At low Ag mole numbers, the SNSFs exist as monomers in small low-density clusters on the filter paper surface. At increased Ag mole numbers, the density and size of these SNSF clusters increase. At high Ag mole numbers, the SNSFs exist as three-dimensional vertical stacks. Multilayered SNSFs comprise aggregate structures measuring several micrometers in size.

**Verification of SNSF-Based SERS Substrates.** To verify the effectiveness of the filter paper-based SERS substrate in strengthening Raman signals, Raman spectra were obtained for the case involving the filter paper-based SERS substrate treated with 2 $\mu$L of 1 mM of rhodamine 6G (R6G) (Figure 4a). The observed strongest R6G peak can be attributed to the aromatic C−C stretching vibrations at 1511 $cm^{-1}$. Moreover, additional aromatic C−C stretching vibration peaks were observed at 1311, 1360, and 1651 $cm^{-1}$ wavelengths,[21] and the peak observed at 1179 $cm^{-1}$ was associated with the in-plane C−H bending vibrations. The observed peak at 1511 $cm^{-1}$ was considered representative of R6G. Figure 4b depicts the intensities of the peak observed at 1511 $cm^{-1}$ as a function of the SNSF Ag mole numbers. As can be seen, minimal strengthening of the Raman signals occurs when the Ag mole number remains below 35.64 $\mu$mol. However, the said signals are considerably strengthened at Ag mole numbers in the 44.55−62.38 $\mu$mol range. At an Ag mole number of 71.29 $\mu$mol, the Raman signal intensities remain nearly constant. Therefore, the SNSF solution considered in this study comprised an Ag mole number of 62.38 $\mu$mol. The enhancement factor (EF) of the SNSF substrate was calculated as follows

$$\mathrm{EF} = \frac{I_{\mathrm{SNSF}}}{I_{\mathrm{O}}} \times \frac{N_{\mathrm{O}}}{N_{\mathrm{SNSF}}}$$

where $I_{\mathrm{SNSF}}$ and $I_{\mathrm{O}}$ are the Raman intensities measured with and without SNSF substrates, respectively. $N_{\mathrm{O}}$ and $N_{\mathrm{SNSF}}$ are the mole numbers of molecules in bulk solution being dripped and adsorbed on the paper without and with SNSF substrates,


https://doi.org/10.1021/acs.analchem.1c02496
Anal. Chem. 2021, 93, 14996−15004

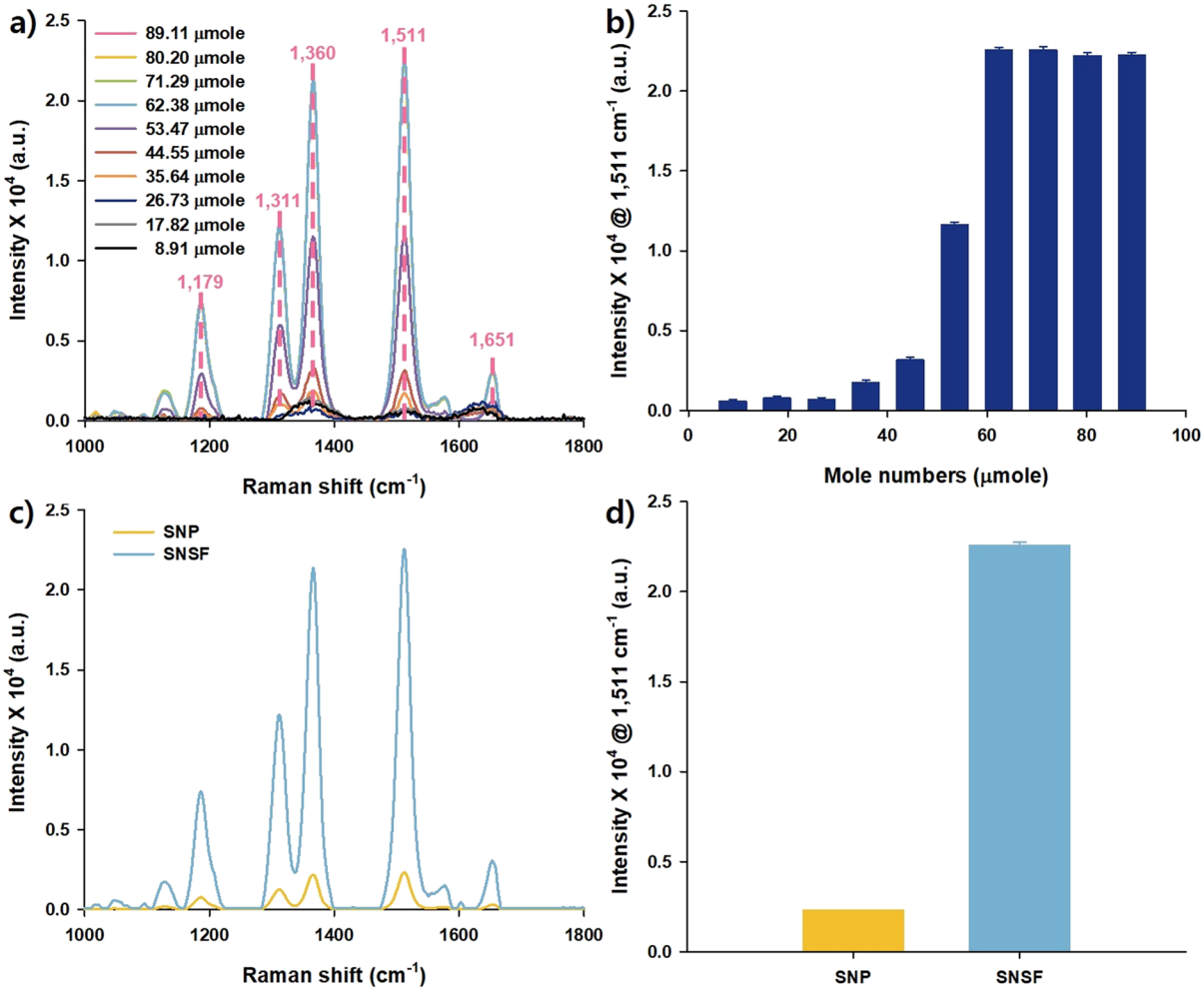


**Figure 4.** (a) Raman spectra for 1 mM rhodamine 6G (R6G) obtained for different Ag mole numbers of SNSF in the SERS substrate, (b) observed 1 mM R6G Raman intensities at 1511 $cm^{-1}$ as a function of substrate Ag mole numbers, (c) Raman spectra, and (d) Raman intensity comparisons between SNSF and SNP at 1511 $cm^{-1}$ wavelengths and identical Ag mole numbers.

respectively. The EF of SNSF substrates can be calculated using data from Figures 4a and S1. The mole numbers of R6G were $2 \times 10^{-9}$ mole (1 mM × 2 μL) when measured with SNSF substrates ($N_{SNSF}$) and $1 \times 10^{-3}$ mole (100 mM × 10 mL) when measured without SNF substrates ($N_O$). The Raman intensities were $I_{SNSF}$ = 22,518.80 and $I_O$ = 1632.18, respectively, and thus, EF is calculated as $6.90 \times 10^6$. Moreover, when comparing the potential of SNSF and SNP (Figure 4c), all signal measurements were performed considering the abovementioned Ag mole number (62.38 μmol). To examine whether hydrophobic treatment on the substrate can enhance Raman signals, SNSF and R6G were dropped on the filter paper-based substrate without hydrophobic treatment. As illustrated in Figure S2, it was confirmed that the Raman signal from R6G could be hardly detected without hydrophobic treatment. To test the SERS activity of the SNSF substrate, EF was calculated using R6G and one of the widely used Raman dyes, Nile Blue A, for both substrates and solutions of SNSF and SNP, respectively (Figure S1). The EF values for each experimental condition were calculated, which are in the similar range of 106 scale (Table S2). To facilitate an accurate comparison between the two spectra depicted in Figure 4c, the observed Raman intensities at 1511 $cm^{-1}$ are replotted in Figure 4d. As can be seen, the Raman intensity for SNSF exceeds that corresponding to SNP by approximately 10 times. This implies that the SNSF-based SERS substrate facilitates high-sensitivity Raman-signal measurements in cases involving small sample volumes (2 μL) using a hand-held Raman spectrometer.

**Detection of Creatinine and Cortisol Using Standard Solution.** To confirm the use of SNSF-based SERS substrates for creatinine and cortisol biomarker detection in human sweat, the corresponding Raman signals were preferentially measured at in vivo biomarker concentrations. To this end, the Raman spectrum of a phosphate-buffered saline (PBS) (Figure 5a) was first obtained. Similar to the previous discussion, 2 μL of solutions containing different analyte concentrations was dropped onto the SNSF-based substrate, and the corresponding Raman spectra were measured. As observed, the standard creatinine solution demonstrated the strongest peak at 632 $cm^{-1}$, owing to the inherent ring vibrations (Figure 5b). The other peaks include those due to $NH_2$ group vibrations observed at wavelengths of 814 and 943 $cm^{-1}$ as well as those caused by the endocyclic C═N and C═O stretching modes[24] prevalent at 1450 $cm^{-1}$. The peak observed at 632 $cm^{-1}$ was considered representative of creatinine because it demonstrated the highest intensity in the obtained Raman spectra. Figure 5c depicts the Raman intensity of the 632 $cm^{-1}$ peak as a function of the creatinine mass. In heatstroke patients, the creatinine concentration in sweat equals or exceeds 1.4 mg/


https://doi.org/10.1021/acs.analchem.1c02496
Anal. Chem. 2021, 93, 14996−15004

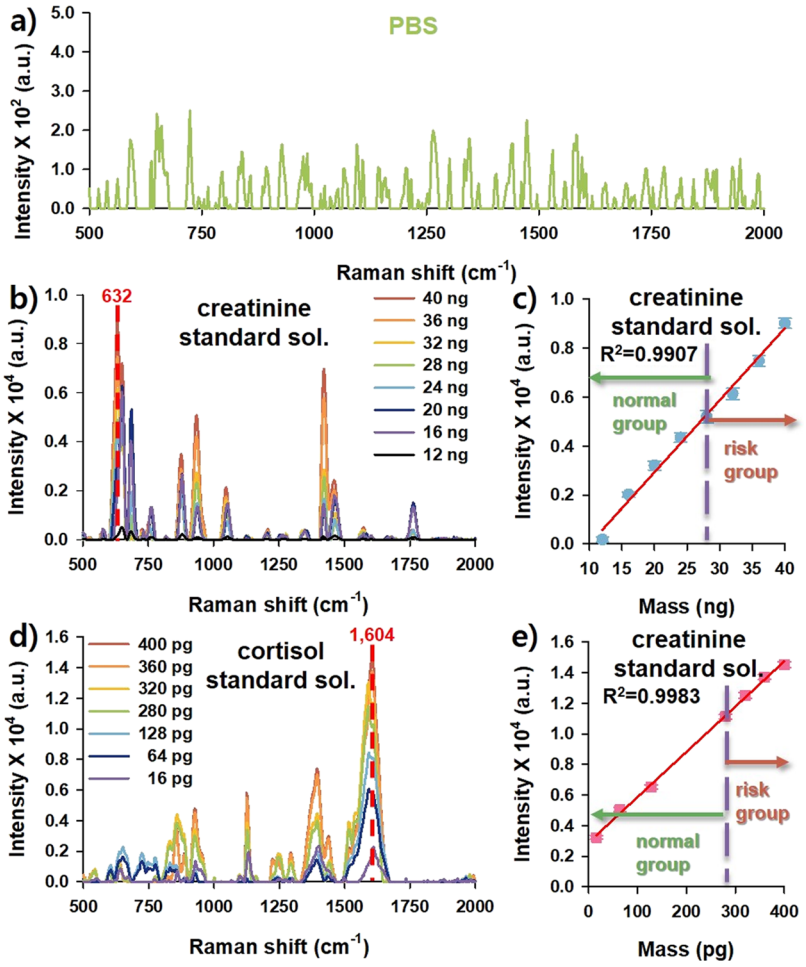


**Figure 5.** (a) Raman spectrum for PBS on the SNSF substrate, (b) Raman spectra for creatinine on the SNSF substrate at varying mass in standard solution, (c) Raman intensity for creatinine at 632 $cm^{-1}$, (d) Raman spectra for cortisol on the SNSF substrate at varying mass in standard solution, and (e) Raman intensity for cortisol at 1604 $cm^{-1}$.

dL,[25] and based on this value, the same could be divided into the normal and at-risk groups. In this study, only 2 $\mu$L of creatinine solution was dropped onto the SNSF-based SERS substrate. Therefore, all concentrations are expressed in terms of mass. In the case involving the cortisol solution, a major Raman peak was observed at 1604 $cm^{-1}$ (Figure 5d). It can be attributed to C═C stretching. Other peaks were observed at 1149 $cm^{-1}$ ($CH_2$ twisting, CH bending, and OH bending), 1239 $cm^{-1}$ (C−C−C asymmetric C-ring stretching), 1275 $cm^{-1}$ (CH bending, $CH_2$ bending, and OH bending), 1346 $cm^{-1}$ (C−C−C symmetric A-ring stretching), and 1382 and 1390 $cm^{-1}$ ($CH_3$ symmetric bending, CH wagging, and OH wagging in C ring).[6] Similar to creatinine, the major peak (1604 $cm^{-1}$) was considered representative of cortisol, and the corresponding Raman intensity was considered a function of the cortisol mass (Figure 5e). The concentration of cortisol in sweat lies in the 8−200 ng/mL range[26] with mental stress causing it to exceed 140 ng/mL.[27] Similar to creatinine, the normal and at-risk groups for cortisol were marked based on the latter concentration. Figure 5c,e depicts Raman intensities of the creatinine and cortisol standard solutions at the selected peaks (632 $cm^{-1}$ for creatinine and 1604 $cm^{-1}$ for cortisol). These intensities were measured with error values of less than 5% when the SNSF-based SERS substrate was used in combination with a hand-held Raman spectrometer.

**Detection of Creatinine and Cortisol in Human Sweat.** To validate the effectiveness of the proposed SNSF-based SERS-substrate and hand-held Raman spectrometer sensor system, Raman signals were acquired from human sweat samples spiked with creatinine and cortisol. To this end, the Raman spectrum of human sweat was first analyzed as a control signal (Figure 6a). As observed, the peak positions in the Raman spectra depicted in Figure 6b are identical to those depicted in Figure 5b. However, the corresponding Raman intensity is decreased by 70%. The observed Raman intensity at 632 $cm^{-1}$ is indicative of the creatinine concentration in human sweat (Figure 6c). However, compared to the standard solution (Figure 5c), the results obtained using the spiked solution are less linear, and the error incurred is larger. Nevertheless, the normal and at-risk groups can be adequately classified. The Raman spectra obtained for the cortisol-spiked human sweat solution are depicted in Figure 6d. As observed, the Raman intensity at 1604 $cm^{-1}$ is indicative of the cortisol concentration (Figure 6e). Similar to Figure 6b, the Raman intensity for cortisol decreases in the human sweat solution (Figure 6d). Furthermore, the observed Raman intensity at 1604 $cm^{-1}$ demonstrates reduced linearity and higher errors (Figure 6e). Despite these weaknesses of spiked human sweat samples, it is confirmed that the normal and at-risk groups can be adequately distinguished using the proposed system. To verify the accuracy of the obtained results in Figure 6,


https://doi.org/10.1021/acs.analchem.1c02496
Anal. Chem. 2021, 93, 14996−15004

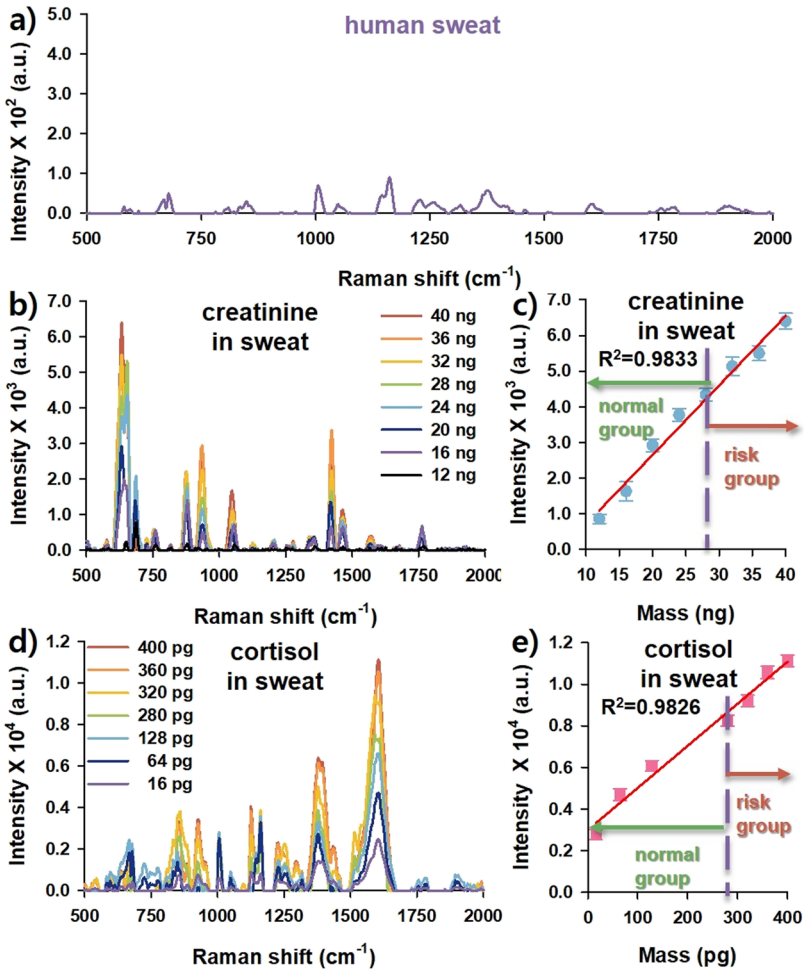


**Figure 6.** (a) Raman spectrum for PBS on the SNSF substrate, (b) Raman spectra for creatinine on the SNSF substrate at varying mass in human sweat, (c) Raman intensity for creatinine at 632 $cm^{-1}$, (d) Raman spectra for cortisol on the SNSF substrate at varying mass in human sweat, and (e) Raman intensity for cortisol at 1604 $cm^{-1}$.

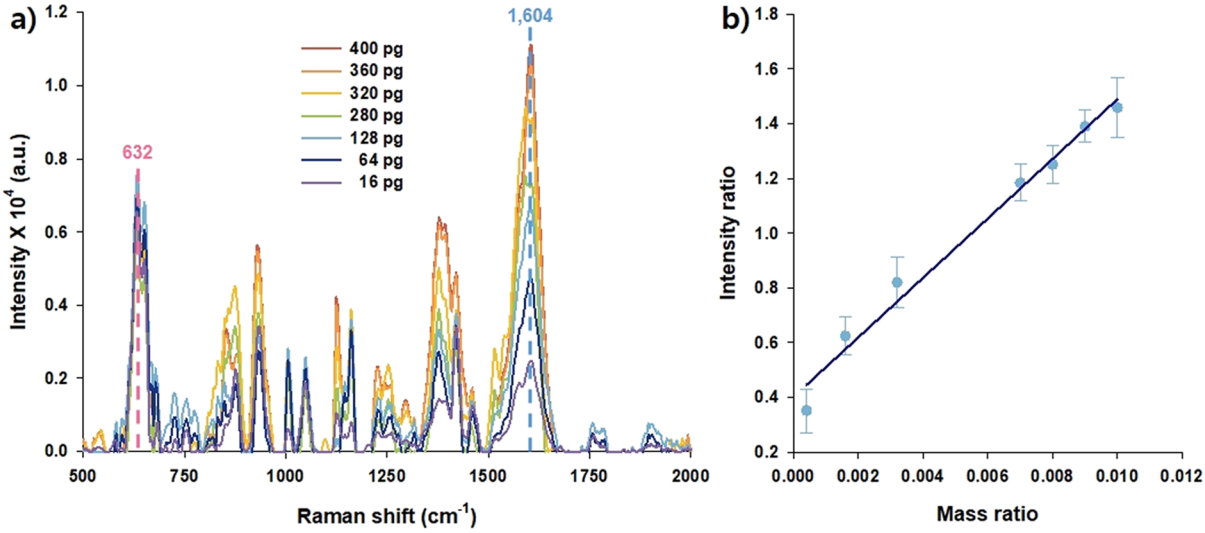


**Figure 7.** (a) Raman spectra for human sweat samples spiked with creatinine (40 ng) and cortisol (16–400 pg) on the SNSF substrate and (b) Raman intensity ratio of cortisol at 1604 $cm^{-1}$ to creatinine at 632 $cm^{-1}$ as a function of mass ratio of cortisol to creatinine in the presence of creatinine (40 ng).

quantitative evaluations of creatinine and cortisol using commercial kits were also conducted, and these results were compared with those acquired from the SNSF-based SERS substrate (Figure S3). The correlation coefficient ($R^2$) between our proposed measurements and results from commercial kits are 0.9792 and 0.9769 for creatinine and cortisol, respectively.


https://doi.org/10.1021/acs.analchem.1c02496
Anal. Chem. 2021, 93, 14996−15004

In addition, to confirm the reproducibility of Raman signals from the SNSF-based SERS substrate, inter-substrate assay has also been conducted. As shown in Figure S4, the tendency of the results does not differ significantly from the results, as shown in Figure 6c,e, and furthermore, the difference in Raman intensity for each mass is more clearly illustrated.

**Multiple Detection of Creatinine and Cortisol in Human Sweat.** The final set of experiments in this study was performed on human sweat solutions spiked with creatinine and cortisol. The Raman spectra obtained for these samples were subsequently analyzed. Because the measurable mass of cortisol equaled approximately 100 times lower compared to that of creatinine, the creatinine mass was fixed (40 ng), while that of cortisol varied, as depicted in Figure 7a. As can be seen, all Raman spectra revealed representative peaks for creatinine (632 $cm^{-1}$) and cortisol (1604 $cm^{-1}$). The variation in the corresponding Raman intensity for creatinine equaled less than 5%, while that in the Raman intensity for cortisol at 1604 $cm^{-1}$ varied according to mass of cortisol. Since the creatinine is present as an internal standard, from the analytical perspective, the Raman intensity ratio of cortisol observed at 1604 $cm^{-1}$ to creatinine observed at 632 $cm^{-1}$ is shown in Figure 7b as a function of the mass ratio of cortisol to creatinine. In addition, after fixing the mass of cortisol (400 pg), Raman signals were also acquired as varying the mass of creatinine (Figure S5). Even in the case when the mass of cortisol was fixed, the Raman intensity for cortisol was almost consistent at 632 $cm^{-1}$. These results indicate that the combination of the SNSF-based SERS substrate and hand-held Raman spectrometer can be used to detect multiple biomarkers. Thus, the cumulative findings of this study demonstrate the potential of the proposed system for use in future liquid-biopsy applications.

## CONCLUSIONS

This paper presents the development of an SNSF-based SERS substrate. Moreover, it reports the assessment of the proposed system's performance to facilitate the accurate detection of creatinine and cortisol in spiked human sweat samples. The findings of this study reveal that a considerable SERS effect can be realized at low sample volumes (2 $\mu$L). The multiple detection potential of the proposed SNSF-based SERS substrate in combination with a hand-held Raman spectrometer is confirmed by the accurate detection and quantification of two biomarkers—creatinine and cortisol—present in human sweat. As a future endeavor, the authors intend to explore the potential of the proposed system for use in liquid-biopsy applications involving other human biofluids, such as blood, saliva, and urine.

## ASSOCIATED CONTENT

### Supporting Information

The Supporting Information is available free of charge at https://pubs.acs.org/doi/10.1021/acs.analchem.1c02496.

Raman spectra as control experiments; comparison between commercial assay kits and our measurement system; box plots for inter-assay reproducibility; multiple biomarker detection with fixed mass of cortisol; comparison of various methods with our measurement system; and enhancement factors of paper-based substrates with rhodamine 6G and Nile Blue A (PDF)

## AUTHOR INFORMATION


### Corresponding Authors

**Gyudo Lee** − *Department of Biotechnology and Bioinformatics, Korea University, Sejong 30019, Republic of Korea; Interdisciplinary Graduate Program for Artificial Intelligence Smart Convergence Technology, Korea University, Sejong 30019, Republic of Korea;* orcid.org/0000-0001-7895-5112; Email: lkd0807@korea.ac.kr

**Yoochan Hong** − *Department of Medical Device, Korea Institute of Machinery and Materials (KIMM), Daegu 42994, Republic of Korea;* orcid.org/0000-0002-6345-9877; Email: ychong1983@kimm.re.kr

### Authors

**Hyun Soo Kim** − *Department of Electronic Engineering, Kwangwoon University, Seoul 01897, Republic of Korea*

**Hyun Jung Kim** − *Department of Medical Device, Korea Institute of Machinery and Materials (KIMM), Daegu 42994, Republic of Korea; Department of Biotechnology and Bioinformatics, Korea University, Sejong 30019, Republic of Korea*

**Jaehun Lee** − *Department of Medical Device, Korea Institute of Machinery and Materials (KIMM), Daegu 42994, Republic of Korea*

**Taeha Lee** − *Department of Biotechnology and Bioinformatics, Korea University, Sejong 30019, Republic of Korea; Interdisciplinary Graduate Program for Artificial Intelligence Smart Convergence Technology, Korea University, Sejong 30019, Republic of Korea*

**Jongsu Yun** − *Department of Medical Device, Korea Institute of Machinery and Materials (KIMM), Daegu 42994, Republic of Korea*

Complete contact information is available at: https://pubs.acs.org/10.1021/acs.analchem.1c02496


### Author Contributions

H.S.K.—conceptualization, methodology, and manuscript preparation. H.J.K.—methodology, data curation, manuscript review, and editing. J.L.—methodology and data curation. T.L.—methodology and visualization. J.Y.—methodology. G.L.—supervision, project administration, manuscript review, and editing. Y.H.—supervision, project administration, manuscript review, and editing. All authors have approved the final version of the manuscript for submission. H.S.K. and H.J.K.—contributed equally to this work.

### Notes

The authors declare no competing financial interest.

## ACKNOWLEDGMENTS

This work is supported by the Korea Institute of Machinery and Materials (KIMM) (NK232D), the Disaster-Safety Industry Promotion Program funded by the Ministry of Interior and Safety (MOIS, Korea) (2019-MOIS32-028), and a National Research Foundation (NRF) of Korea grant (NRF-2018R1A6A1A03025242, NRF-2021R1C1C1012822, and NRF-2021R1F1A1063455) funded by the Korean government. This research is also funded by the Korea Medical Device Development Fund grant received from the Korean government (the Ministry of Science and ICT, Project Number: 202012D19). In addition, this work is funded by the Research Resettlement Fund for the new faculty of the Kwangwoon University in 2021.

## REFERENCES


(1) Im, Y. R.; Tsui, D. W. Y.; Diaz, L. A.; Wan, J. C. M. *Trends Cancer Res.* **2021**, *7*, 283−292.
(2) De Rubis, G.; Rajeev Krishnan, S.; Bebawy, M. *Trends Pharmacol. Sci.* **2019**, *40*, 172−186.
(3) Wang, J.; Chang, S.; Li, G.; Sun, Y. *Front. Med.* **2017**, *11*, 522−527.
(4) Zhang, Y.; Guo, H.; Kim, S. B.; Wu, Y.; Ostojich, D.; Park, S. H.; Wang, X.; Weng, Z.; Li, R.; Bandodkar, A. J.; et al. *Lab Chip* **2019**, *19*, 1545−1555.
(5) Bernal-Reyes, F.; Acosta-Elias, M.; Burgara-Estrella, A. J.; Álvarez-Bajo, O.; Gavotto-Nogales, O. I.; Antunez-Dominguez, F. J.; Placencia-Camacho, L.; Sarabia-Sainz, H. M. *Instrum. Sci. Technol.* **2020**, *48*, 361−375.
(6) Moore, T. J.; Sharma, B. *Anal. Chem.* **2020**, *92*, 2052−2057.
(7) Appel, D.; Schmid, R. D.; Dragan, C.-A.; Bureik, M.; Urlacher, V. B. *Anal. Bioanal. Chem.* **2005**, *383*, 182−186.
(8) Zangheri, M.; Cevenini, L.; Anfossi, L.; Baggiani, C.; Simoni, P.; Di Nardo, F.; Roda, A. *Biosens. Bioelectron.* **2015**, *64*, 63−68.
(9) Jo, S.; Lee, W.; Park, J.; Kim, W.; Kim, W.; Lee, G.; Lee, H.-J.; Hong, J.; Park, J. *Sens. Actuators, B* **2020**, *304*, 127424.
(10) Kim, Y.-H.; Lee, K.; Jung, H.; Kang, H. K.; Jo, J.; Park, I.-K.; Lee, H. H. *Biosens. Bioelectron.* **2017**, *98*, 473−477.
(11) Sun, B.; Gou, Y.; Ma, Y.; Zheng, X.; Bai, R.; Ahmed Abdelmoaty, A. A.; Hu, F. *Biosens. Bioelectron.* **2017**, *88*, 55−62.
(12) Langer, J.; Jimenez de Aberasturi, D.; Aizpurua, J.; Alvarez-Puebla, R. A.; Auguié, B.; Baumberg, J. J.; Bazan, G. C.; Bell, S. E. J.; Boisen, A.; Brolo, A. G.; et al. *ACS Nano* **2020**, *14*, 28−117.
(13) Kim, H. S.; Lee, T.; Yun, J.; Lee, G.; Hong, Y. *Microchem. J.* **2021**, *160*, 105632.
(14) Jeanmaire, D. L.; Van Duyne, R. P. *J. Electroanal. Chem. Interfacial Electrochem.* **1977**, *84*, 1−20.
(15) Gahlaut, S. K.; Savargaonkar, D.; Sharan, C.; Yadav, S.; Mishra, P.; Singh, J. P. *Anal. Chem.* **2020**, *92*, 2527−2534.
(16) Ding, Q.; Zhang, L.; Yang, L. *Mater. Res. Bull.* **2014**, *53*, 205−210.
(17) Reilly, T. H.; Corbman, J. D.; Rowlen, K. L. *Anal. Chem.* **2007**, *79*, 5078−5081.
(18) Marquestaut, N.; Martin, A.; Talaga, D.; Servant, L.; Ravaine, S.; Reculusa, S.; Bassani, D. M.; Gillies, E.; Lagugné-Labarthet, F. *Langmuir* **2008**, *24*, 11313−11321.
(19) Lee, M.; Oh, K.; Choi, H.-K.; Lee, S. G.; Youn, H. J.; Lee, H. L.; Jeong, D. H. *ACS Sens.* **2018**, *3*, 151−159.
(20) Garcia-Leis, A.; Rivera-Arreba, I.; Sanchez-Cortes, S. *Colloid. Surface. Physicochem. Eng. Aspect.* **2017**, *535*, 49−60.
(21) Kim, H. S.; Lee, T.; Yun, J.; Lee, G.; Hong, Y. *Microchem. J.* **2021**, *160*, 105632.
(22) Shameli, K.; Ahmad, M. B.; Zamanian, A.; Sangpour, P.; Shabanzadeh, P.; Abdollahi, Y.; Zargar, M. *Int. J. Nanomed.* **2012**, *7*, 5603−5610.
(23) Taylor, R. W.; Esteban, R.; Mahajan, S.; Aizpurua, J.; Baumberg, J. J. *J. Phys. Chem. C* **2016**, *120*, 10512−10522.
(24) Gangopadhyay, D.; Sharma, P.; Singh, S. K.; Singh, P.; Deckert, V.; Popp, J.; Singh, R. K. *RSC Adv.* **2016**, *6*, 58943−58949.
(25) Alzeer, A. H.; Al Otair, H. A. K. *J. Taibah Univ. Medical Sci.* **2014**, *9*, 50−53.
(26) Munje, R. D.; Muthukumar, S.; Panneer Selvam, A.; Prasad, S. *Sci. Rep.* **2015**, *5*, 14586.
(27) Tu, E.; Pearlmutter, P.; Tiangco, M.; Derose, G.; Begdache, L.; Koh, A. *ACS Omega* **2020**, *5*, 8211−8218.




https://doi.org/10.1021/acs.analchem.1c02496
*Anal. Chem.* 2021, 93, 14996−15004